ACS OMEGA

http://pubs.acs.org/journal/acsodf

Article

Sour Gas Adsorption on Silica Gels

John H. Jacobs, Kaylan H. McKelvie, Safeer Nanji, and Robert A. Marriott*

Cite This: *ACS Omega* 2023, 8, 12592−12602

Read Online

ACCESS | Metrics & More | Article Recommendations | Supporting Information

ABSTRACT: One of the essential factors for water adsorption on silica gels is the concentration of silanol groups on the silica surface. However, no systematic investigation on the adsorption of sour gas components, methane (CH_4), carbon dioxide (CO_2), and hydrogen sulfide (H_2S) on silica gels with different textural properties and surface silanol concentrations, has been conducted. Three silica gels of 22, 30, and 60 Å pore sizes, with silanol concentrations of α_{total} = 2.516, 2.340, and 2.152 OH nm^{-2}, respectively, were studied in this work. The adsorption data for CH_4, CO_2, H_2S, and H_2O at T = 0, 25, and 50 °C on the 22 and 30 Å pore size silica gels were presented, and a comparison of the data for the 60 Å pore size silica gel on the same adsorbates was conducted. All three silica gels showed an adsorption affinity in the order of H_2O > H_2S > CO_2 > CH_4. The isosteric heats of adsorption of H_2O and H_2S had a greater dependence on the silanol concentration than CO_2 and CH_4. At p < 10 bar, there was no difference in the adsorption per m^2 of CH_4 between the silica gels (n^{ads} = 1.7 mmol m^{-2}, for all silicas at p = 10 bar), while higher pressures resulted in greater adsorption capacity in the larger pore volume silica gels (at p = 20 bar: n^{ads} = 3.0, 3.3, and 3.4 mmol m^{-2} for the 22, 30, and 60 Å pore size silicas, respectively). H_2S adsorption at low pressures (p < 4 bar) was larger on the samples with larger silanol concentrations (at p = 3 bar: n^{ads} = 6.1, 4.7, and 4.5 mmol m^{-2} for the 22, 30, and 60 Å pore size silicas, respectively), but above p = 4 bar, the 60 Å pore size silica had a greater adsorption capacity than the 30 Å pore size (at p = 5 bar: n^{ads} = 8.0, 6.0, and 6.2 mmol m^{-2} for the 22, 30, and 60 Å pore size silicas, respectively).

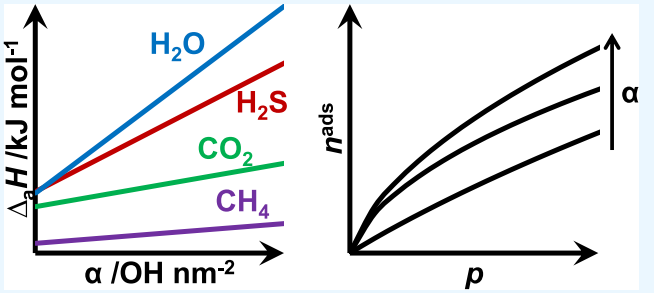

1. INTRODUCTION

Water removal from natural gas is a necessary industrial process for mitigating pipeline corrosion, avoiding hydrate formation within transportation lines, and avoiding solids within liquefaction. Absorption by glycol is the favored technology for removing water from natural gas, but solid desiccants are preferred when low dew points are required (such as in cryogenic systems) or in remote locations where space is limited (such as off-shore rigs). Silica gels are a common desiccant choice as they can reach lower dew points than glycol units and are inexpensive compared to hygroscopic zeolites.[1]

It is well known that water adsorption on silica gels is impacted by the concentrations of silanol groups on the surface of the material.[2] Water molecules will hydrogen bond with the exposed silanol groups, which therefore increases the affinity of the surface to water. Thermal treatment of silica gels can reduce silanol concentrations, while treatment with water will regenerate or even add additional silanol groups to the surface of silica gels.[2,3] Further investigation into water adsorption on silica gels indicates that the silanol groups are expected to be the most important factor for water adsorption rather than varying pore sizes of silica gels.[4]

While the impact of silanol groups on water adsorption has been readily studied for the past few decades, there are limited investigations on how silica functionality impacts the adsorption of other components of natural gas. Note that natural gas is primarily composed of methane (CH_4) but can also contain carbon dioxide (CO_2), hydrogen sulfide (H_2S), water (H_2O), and heavier hydrocarbons (ethane, propane, butane, etc.).[5] Of interest, Kim and Jang conducted a molecular simulation study on the adsorption of CO_2 on amorphous silica surfaces.[6] The authors demonstrated that water adsorption on silica reduces the adsorption of CO_2,[6] an effect also observed in experimental systems.[7] Furthermore, lowering the silanol concentration on the silica surface reduced the amount of CO_2 adsorbed.[6] Another molecular dynamics simulation by Mohammed et al.[8] showed that CO_2 and CH_4 both preferred the silanol sites over CH_3-terminated silica surfaces. These computational studies support increasing the silanol concentration to increase the affinity of natural gas components to silica surfaces.

While computational studies indicate that increasing the surface silanol concentrations of silica gels would increase the affinity of CO_2 and CH_4 to the silica, no lab-scale experiments

Received: February 28, 2023
Accepted: March 9, 2023
Published: March 22, 2023

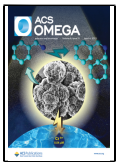

Table 1. Surface Area, Porosity, and Silanol Concentrations of the Three Silica Gels

	22 Å pore size silica	30 Å pore size silica	60 Å pore size silica
$A_{BET}/m^2\ g^{-1}$	641 ± 12	470 ± 2	453.5 ± 0.6
$A_{micropore.\ t\text{-plot}}/m^2\ g^{-1}$	201		
$V_{pore}/cm^3\ g^{-1}$	0.40	0.52	1.07
$V_{micropore.\ t\text{-plot}}/cm^3\ g^{-1}$	0.10		
δ_{total}/mmol g^{-1}[a]	2.678 ± 0.001	1.828 ± 0.005	1.621 ± 0.004
α_{total}/OH nm^{-2}[b]	2.516 ± 0.001	2.340 ± 0.006	2.152 ± 0.006
$\alpha_{vicinal}$/OH nm^{-2}	0.8793 ± 0.0004	0.471 ± 0.001	0.489 ± 0.001
$\alpha_{geminal+isolated}$/OH nm^{-2}	1.6371 ± 0.0008	1.869 ± 0.005	1.663 ± 0.005

[a]The silanol concentration as mmol g^{-1}. [b]The silanol concentration normalized to the number of silanols per nm^2.

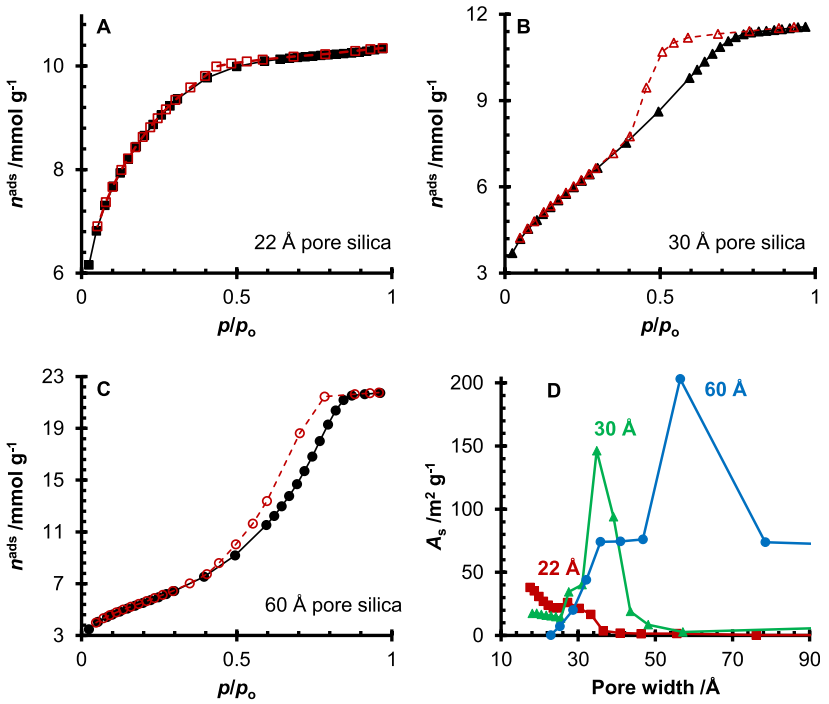

Figure 1. N_2 adsorption isotherms at T = 77 K for the 22 (A), 30 (B), and 60 Å (C) pore size silica gels. For (A−C), black symbols (solid black lines) represent adsorption and red symbols (dashed red lines) represent desorption. The A_s versus pore width plot for the 22 Å (red. □), 30 Å (green, Δ), and 60 Å (blue, ○) pore size silica gels (D). For all four graphs, the lines connecting the points guide the eye.

have investigated these correlations.[9] Correlations for the adsorption of H_2S on a silica surface are uncommon and only one study reports the isosteric heat of adsorption for H_2S on a silica gel in the literature. Additionally, H_2S is a difficult species to work with due to the inherent toxicity of the fluid;[10] thus, adsorption experiments with pure H_2S are uncommon. Investigations into the adsorption behavior of the major components of natural gas are important for modeling applications, where multicomponent adsorption models can be used to estimate the separation of mixtures on an adsorbent bed.

In this work, the adsorption of the natural gas components H_2S, CH_4, and CO_2 was measured using a manometric adsorption instrument on two silica materials. The isosteric heats of adsorption and the adsorption capacities of H_2S, CH_4, CO_2, and H_2O of different silica materials were compared to the silanol concentration of the silica gels and results on how the porosity, specific surface area, and silanol concentration of the silica gels impact the adsorption of the different components were discussed.

2. RESULTS AND DISCUSSION

2.1. Material Characterization. The specific surface area, porosity, and silanol concentration of the three silica gels are reported in Table 1. As expected, the 22 Å pore size silica has the greatest specific surface area of the three silica gels, and it is the only silica gel with a measured microporosity from the *t*-plot. In addition, TGA of silanol groups on the silica surface showed that the 22 Å pore size silica had the greatest concentration of silanol groups. When the N_2 physisorption of the silica gels was analyzed, the 22 Å pore size silica showed a type I isotherm (Figure 1A), while the 30 and 60 Å pore size silicas showed type IV isotherms (Figure 1B,C). All three silica gels showed hysteresis during the desorption, but the 22 Å pore size silica showed minimal hysteresis around p/p_o = 0.4−0.5. The hysteresis loop of the 30 Å pore silica gel resembles the H2(a) type, typical of silica gels with a complex pore structure.[11] The 60 Å pore silica showed a type H1 hysteresis loop, typical of uniform mesopores.[11] From the distribution of surface area over the different pore sizes, as shown in Figure 1D, there is a clear maximum surface area for the 30 and 60 Å pore size silicas at w_{pore} = 35 Å and w_{pore} = 56 Å, respectively.

https://doi.org/10.1021/acsomega.3c01366
ACS Omega 2023, 8, 12592−12602

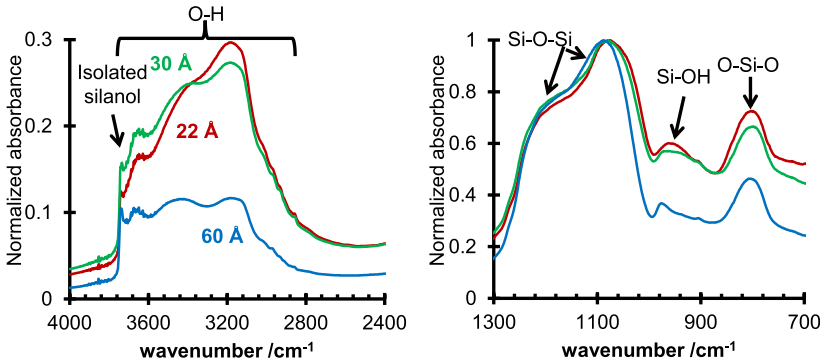

Figure 2. DRIFT spectra of the 22 Å (red), 30 Å (green), and 60 Å (blue) silica gels.

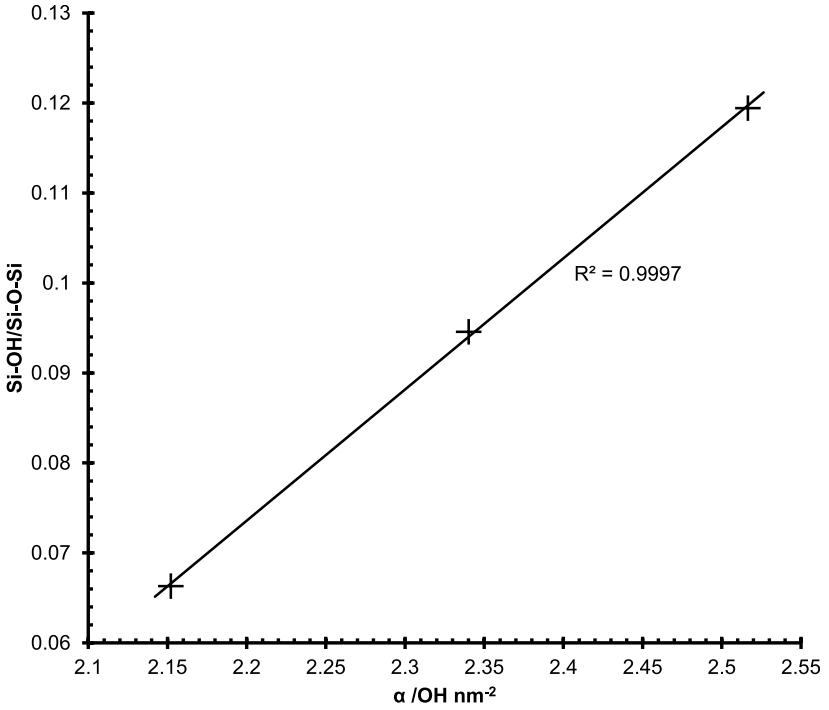

Figure 3. atios of Si−OH (∼950 cm^{-1}) and Si−O−Si (∼1100 cm^{-1}) vs the silanol number of the three silica gels. The solid line indicates a linear fit.

In contrast, the 22 Å pore size silica continues to increase in the micropore region. The number of silanol groups per nm^2 (α_{total}) for the three silica gels is in the range of α_{total} = 2.152−2.516 OH nm^{-2}, which is lower than Zhuravlev's number of α_{total} = 4.9 OH nm^{-2} for the average silanol concentration on silica gels.[12]

All three silica gels showed an isolated silanol peak at ∼3740 cm^{-1} in the diffuse reflectance infrared Fourier transform (DRIFT) spectra (Figure 2).[3] Interestingly, there are three peaks within the OH stretching range at 3120−3280, 3360−3520, and ∼3680 cm^{-1} for all three silica gels, but with varying peak heights between materials which likely correspond to hydrogen bonding of adsorbed water to different adsorption sites. The Si−O−Si peaks were observed in the range of 1060−1100 and ∼1220 cm^{-1}.[13] The 60 Å pore size silica had the smallest silanol peak at ∼980 cm^{-1} of the three silicas, while the 22 and 30 Å pore size silicas showed similar shapes and sizes for the silanol peak. A qualitative assessment of the DRIFT results indicates that the 60 Å pore size silica has the least number of silanol groups of the three silica gels. The 22 and 30 Å pore silicas showed similar DRIFT spectra. Analysis of the silanol concentration of the three silica gels was done by comparing the ratio of the maximum peaks for the silanol groups (∼980 cm^{-1}) with the bulk silica (∼1100 cm^{-1}). Comparing the Si−OH/Si−O−Si ratio from the DRIFT spectra with the silanol numbers from the TGA experiments shows a linear correlation with an R^2 = 0.9997 between the two methods, indicating agreement between the two techniques for the silanol concentrations (Figure 3).

2.2. Adsorption Isotherms. The adsorption isotherms of CH_4 (Figure 4), CO_2 (Figure 5), and H_2S (Figure 6) are shown in Figures 4−6 for the 22, 30, and 60 Å pore size silica gels. The fitting parameters for the modified Tóth equation are presented in Table 2, and the isosteric heats of adsorption are presented in Table 3. The adsorption isotherms for the 60 Å pore size silica gel were collected previously by Wynnyk et al.[9] on the same adsorption instrument and the data were refit for the modeling used in this work. The adsorption affinity for the sour gas components on all three silica gels followed the H_2O > H_2S > CO_2 > CH_4 order. Silanol groups are polar moieties

https://doi.org/10.1021/acsomega.3c01366
ACS Omega 2023, 8, 12592−12602

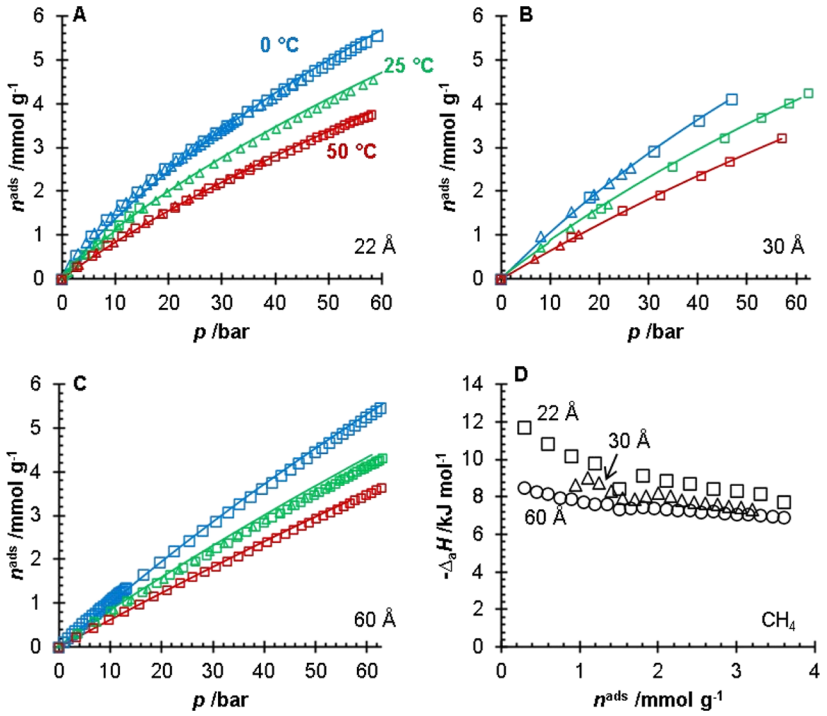

Figure 4. CH_4 adsorption isotherms (A–C) for the 22 (A), 30 (B), and 60 Å (C) pore size silica gels. For (A–C) the different symbols (□, Δ) represent replicates of the experiments and the lines represent a fitted modified Tóth equation collected at T = 0 °C (blue), 25 °C (green), and 50 °C (red). The isosteric heats of adsorption (D) of CH_4 for the 22 Å (black, □), 30 Å (black, Δ), and 60 Å (black, ○) pore size silica gels. The data for the 60 Å pore size silica gel were obtained and replotted from the work of Wynnyk et al.[9]

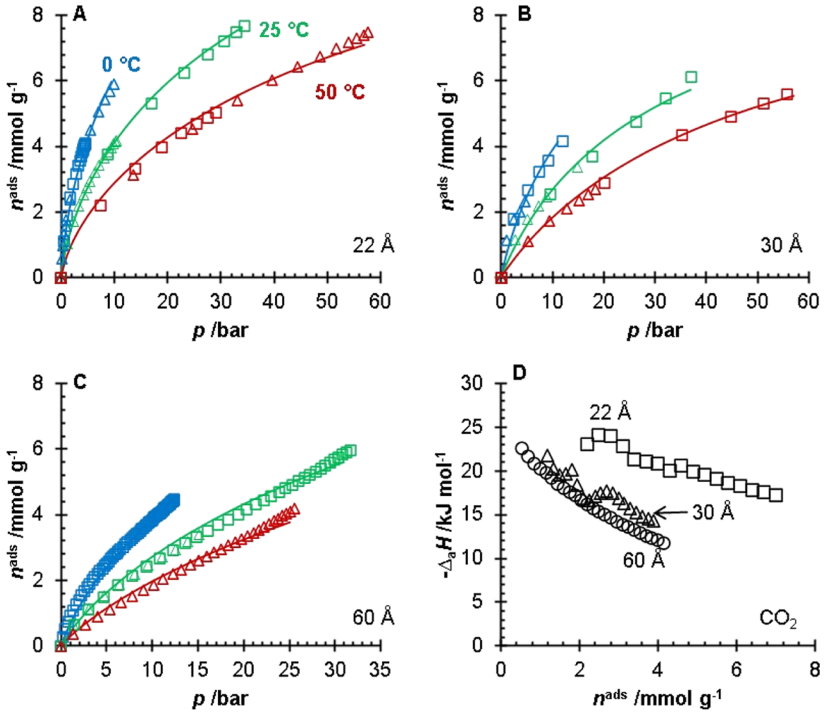

Figure 5. CO_2 adsorption isotherms (A–C) for the 22 (A), 30 (B), and 60 Å (C) pore size silica gels. For (A–C) the different symbols (□, Δ) represent replicates of the experiments and the lines represent a fitted modified Tóth equation collected at T = 0 °C (blue), 25 °C (green), and 50 °C (red). The isosteric heats of adsorption (D) of CO_2 for the 22 Å (black, □), 30 Å (black, Δ), and 60 Å (black, ○) pore size silica gels. The data for the 60 Å pore size silica gel were obtained and replotted from the work of Wynnyk et al.[9]

capable of hydrogen bonding with species such as H_2O. Due to polarity and polarizability, it is reasonable that the H_2S molecules would have stronger interactions with the silanol groups than the non-polar and relatively unpolarizable CO_2 and CH_4 molecules. The data on H_2S, CO_2, and CH_4 adsorption for the 22 and 30 Å pore size silica gels are presented in the Supporting Information; this included the uncertainties of the measurements. The water adsorption data

https://doi.org/10.1021/acsomega.3c01366
ACS Omega 2023, 8, 12592−12602

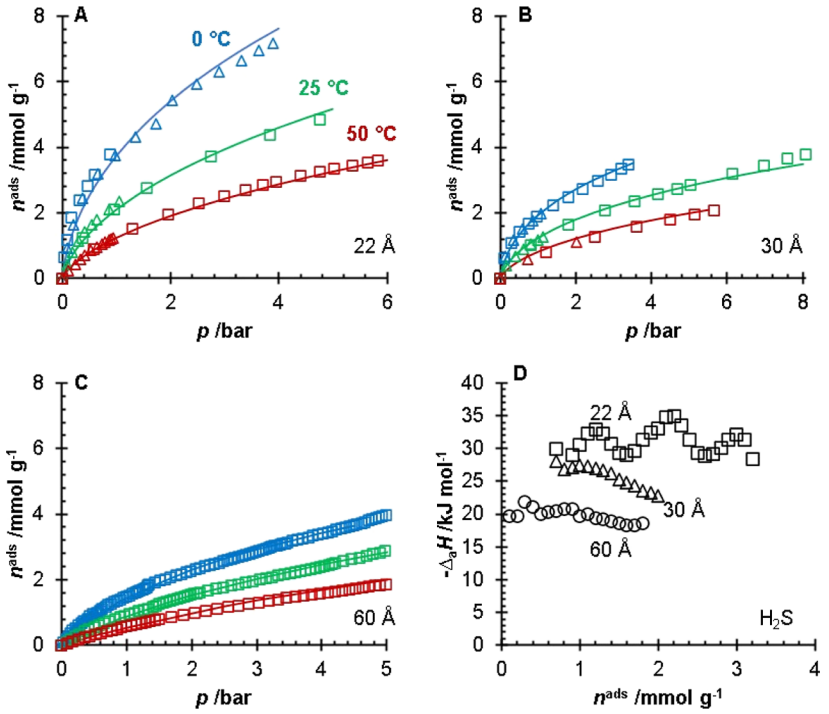

Figure 6. H_2S adsorption isotherms (A−C) for the 22 (A), 30 (B), and 60 Å (C) pore size silica gels. For (A−C) the different symbols (□, Δ) represent replicates of the experiments and the lines represent a fitted modified Tóth equation collected at T = 0 °C (blue), 25 °C (green), and 50 °C (red). The isosteric heats of adsorption (D) of H_2S for the 22 Å (black, □), 30 Å (black, Δ), and 60 Å (black, ○) pore size silica gels. The data for the 60 Å pore size silica gel were obtained and replotted from the work of Wynnyk et al.[9]

Table 2. Fitting Parameters for the Modified Tóth Equation

pore size	fluid	n^{∞}/mmol g^{-1}	$b°$/bar^{-1}	-$\Delta H_{Tóth}$/kJ mol^{-1}	A	B/K^{-1}	MSSE
22 Å	CH_4	4.58×10^2	7.42×10^{-6}	9.20	2.46×10^{-1}	4.28×10^{-4}	4.60×10^{-3}
	CO_2	5.57×10^2	4.29×10^{-6}	20.39	1.70×10^{-1}	2.89×10^{-5}	1.71×10^{-2}
	H_2S	17.46	1.05×10^{-5}	26.69	6.46×10^{-1}	-7.68×10^{-4}	6.9×10^{-3}
	H_2O[15]	35.12	2.33×10^{-5}	34.9	9.02	-1.98×10^{-5}	
30 Å	CH_4	29.04	1.12×10^{-4}	7.99	9.67×10^{-1}	1.03×10^{-4}	6.77×10^{-3}
	CO_2	17.93	2.09×10^{-5}	17.43	2.09×10^{-1}	1.57×10^{-3}	3.24×10^{-2}
	H_2S	73.50	1.09×10^{-5}	25.30	1.69×10^{-1}	1.10×10^{-4}	1.37×10^{-2}
	H_2O[15]	22.88	1.38×10^{-4}	30.2	3.07	-5.26×10^{-3}	
60 Å	CH_4	3.44×10^2	1.08×10^{-5}	7.46	1.00	2.12×10^{-4}	7.25×10^{-3}
	CO_2	2.00×10^2	4.64×10^{-6}	16.55	1.74×10^{-1}	4.70×10^{-4}	1.08×10^{-2}
	H_2S	11.20	3.48×10^{-5}	19.77	-7.64×10^{-2}	2.64×10^{-3}	4.75×10^{-3}
	H_2O	4.40×10^5	3.34×10^{-4}	18.42	9.99×10^{-2}	-7.50×10^{-5}	1.52×10^{-2}

Table 3. Isosteric Heats of Adsorption of the Silica Gels

$\Delta_a H$/kJ mol^{-1}	loading/mmol g^{-1}	H_2O	CH_4	CO_2	H_2S
Literature		48,[16] 47.9,[17] 45.6[18]	10.30,[19] 6.6,[20] 14.873[21]	22.3,[19] 24.967[21]	
22 Å	0	34.78 ± 0.04[a]	12.5 ± 0.3	26.8 ± 0.4	31.3 ± 1.1
	1.5	34.78 ± 0.04[a]	8.7 ± 0.2	24.7 ± 0.4	31.2 ± 1.1
30 Å	0	30.66 ± 0.06[a]	9.3 ± 0.2	23.4 ± 0.5	31.1 ± 0.5
	1.5	30.20 ± 0.06[a]	8.4 ± 0.1	19.9 ± 0.5	25.2 ± 0.4
60 Å	0	23.3 ± 1.6[b]	8.2 ± 0.1[b]	23.4 ± 0.3[b]	21.1 ± 0.3[b]
	1.5	18.7 ± 1.3[b]	7.6 ± 0.1[b]	18.9 ± 0.2[b]	19.0 ± 0.3[b]

[a]Fit from the data of Jacobs et al.[15] [b]Fit from the data of Wynnyk et al.[9]

for the 22 and 30 Å pore size silica gels and the adsorption of H_2S, CO_2, CH_4, and H_2O for the 60 Å pore size silica gel have been previously reported in the literature.[9,14]

The isosteric heat of adsorption for water was lower than the literature values. The CO_2 isosteric heat measured on the silica gels in this work overlaps with the values reported in the literature. The CH_4 isosteric heat is within the range reported in the literature (Table 3). Differences in silanol concentrations can explain the different experimental and literature values in the isosteric heats presented in Table 3. It should be noted that the only study we could find reporting the isosteric heat for H_2S on silica gel was the work of Wynnyk et al.[9]

https://doi.org/10.1021/acsomega.3c01366
ACS Omega 2023, 8, 12592−12602

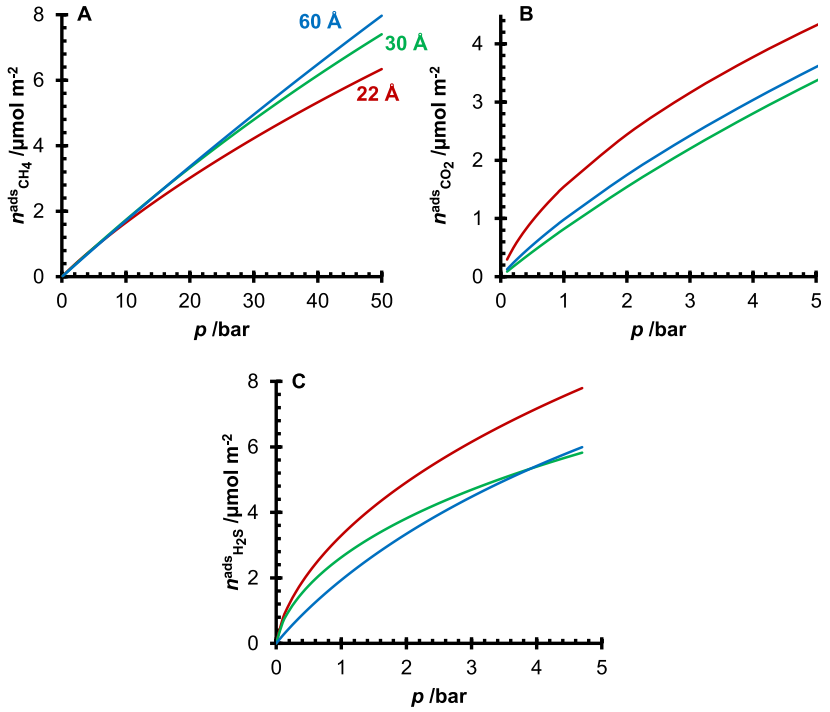

Figure 7. Modeled adsorption isotherms of CH_4 (A), CO_2 (B), and H_2S (C) on the 22 Å (red), 30 Å (green), and 60 Å (blue) pore size silica gels.

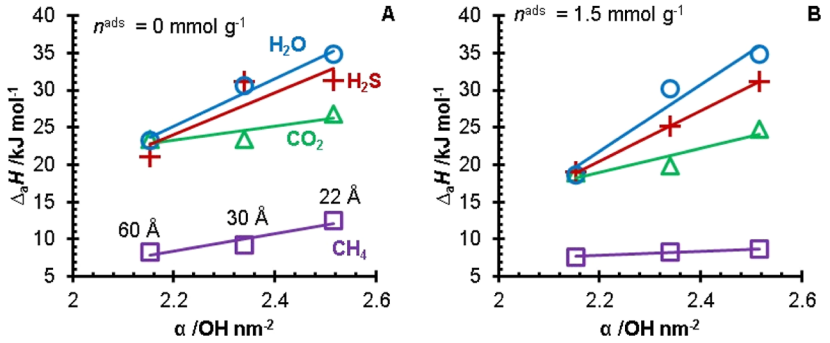

Figure 8. sosteric heats of adsorption at n^{ads} = 0 mmol g^{-1} (A) and n^{ads} = 1.5 mmol g^{-1} (B) for H_2O (blue, ○) as reported in the literature, H_2S (red, +), CO_2 (green, Δ), and CH_4 (purple, □) versus the silanol concentrations of the three silica gels. The heats of adsorption for the 60 Å pore size silica were calculated from the data of Wynnyk et al.[15] The H_2O heats of adsorption for the 22 and 30 Å pore size silicas were calculated from the data of Jacobs et al.[9] Solid lines indicate linear fits.

reported for the 60 Å pore size silica gel, which was used and discussed in this work.

2.3. Adsorption Trends. The amount of adsorbed CH_4, CO_2, and H_2S was modeled using the fitted modified Tóth equation at T = 25 °C and shows specific to surface area versus mass (mmol m^{-2} instead of mmol g^{-1}) in Figure 7. Surface specific adsorption was plotted to highlight the influence of the silanol concentrations on the adsorption of the four sour gas components. Figure 7A shows no significant difference in the CH_4 adsorption below p = 10 bar. However, at higher pressures, it is observed that the amount of CH_4 adsorbed on the surface is perhaps weakly related to the silanol concentrations of the three silicas, where the 60 Å pore size silica has the highest capacity. In contrast, the 22 Å pore size silica has the lowest capacity. In the literature, it has been shown that, on carbon surfaces, changes in the functional group concentrations can change the bulk attraction of molecules to the surface.[22,23] Important factors from the computational analysis are the size of the adsorbates and the intermolecular forces (dipole moments and polarizabilities of the molecules).

A plot of the isosteric heats of adsorption versus the surface silanol concentrations of the three silica gels is presented in Figure 8 to evaluate the influence of the silanol groups on the adsorption of sour gas components. For all four components, the enthalpy of adsorption increased with the silanol concentration. The isosteric heat versus silanol concentration slope was greatest for water, followed by H_2S, CO_2, and CH_4. The difference in slopes shows that the stronger interactions of hydrogen bonding (H_2O) and polarizability (H_2S) with the silica surface are greater than non-hydrogen bonding and low polarizable molecules such as CH_4. A computational study by Kim et al.[24] investigated the adsorption of H_2S on α-quartz surfaces. The computations demonstrated that cleaved silica was the preferred adsorption site for H_2S. The largest concentration of uncoordinated active sites on the silica surface will be the edges of the silica pores. It would then stand to reason that a more porous silica gel would have a greater

https://doi.org/10.1021/acsomega.3c01366
ACS Omega 2023, 8, 12592−12602

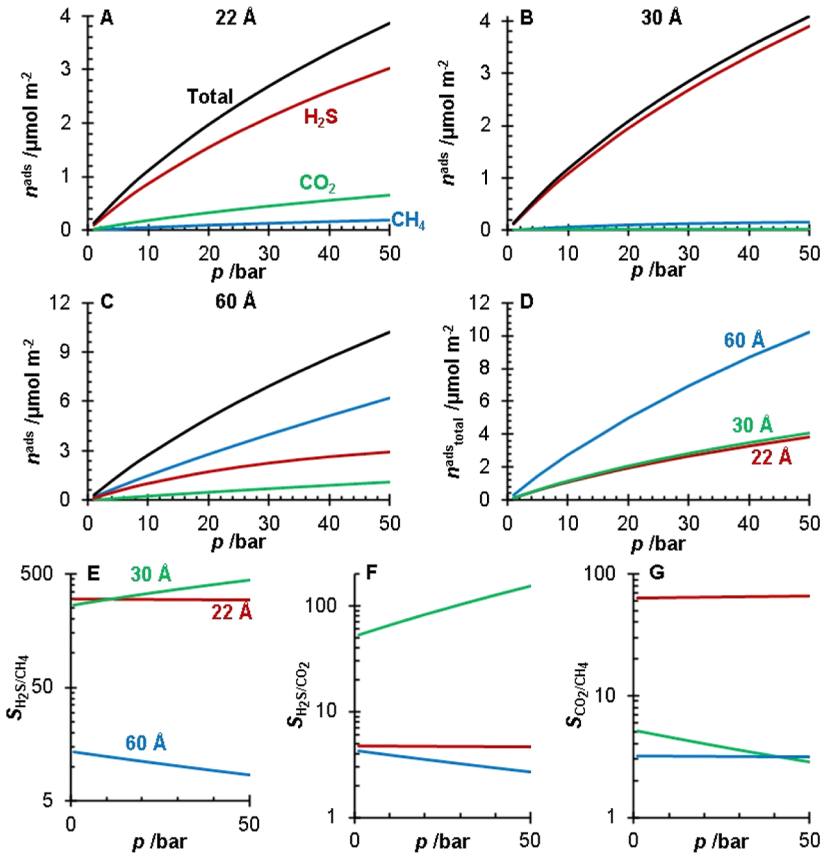

Figure 9. IAST calculations for a 0.9:0.05:0.05 $CH_4/CO_2/H_2S$ gas mixture at T = 25 °C and p = 1−50 bar for the 22 (A), 30 (B), and 60 Å (C) pore size silicas. For graphs (A−C), the total amount adsorbed (black) and the amounts adsorbed of CH_4 (blue), CO_2 (green), and H_2S (red) are presented. Graph (D) compares the total amount adsorbed for the 22 Å (red), 30 Å (green), and 60 Å (blue) pore size silicas. The H_2S/CH_4 (E), H_2S/CO_2 (F), and CO_2/CH_4 (G) selectivities for the 22 Å (red), 30 Å (green), and 60 Å (blue) pore size silicas are reported.

concentration of active sites (geminal silanol groups) and thus have a greater affinity for H_2S. This observation is supported by Figure 8, where the larger concentration of silanol groups results in a larger isosteric heat of adsorption.

It should be noted that of the three silica gels, the 60 Å pore size silica has the largest pore volume, while the 22 Å has the smallest. Thus, it is likely that at pressures greater than p = 10 bar, the adsorption mechanism (for CH_4) becomes a volume-filling mechanism over a surface coverage mechanism. In Figure 7B (CO_2 adsorption), the 60 Å pore size silica gel had a greater capacity than the 30 Å. However, relative to the 22 Å pore size silica, the capacities of the 30 and 60 Å pore size silicas were similar. For the H_2S adsorption (Figure 7C), the 30 Å pore size silica gel had a greater capacity than the 60 Å pore size silica gel until around p = 4 bar, where the 60 Å pore size silica gel had a higher amount of adsorbed H_2S. The crossover in the amount of adsorbed H_2S is likely due to the larger pore volume of the 60 Å pore silica gel.

2.4. Multicomponent Adsorption Modeling. Multicomponent adsorption of a 0.9:0.05:0.05 $CH_4/CO_2/H_2S$ was calculated using the fitted modified Tóth equations for the silica gels determined above. The multicomponent adsorption calculations were conducted using the Ideal Adsorbed Solution Theory (IAST) of Myers and Prausnitz.[25] The multicomponent adsorption was calculated at T = 25 °C over the p = 1−50 bar pressure range. The results of the IAST calculations are presented in Figure 9. The IAST calculations show that the 22 and 30 Å pore size silicas adsorb more H_2S than CH_4 or CO_2, while the 60 Å pore size silica adsorb more CH_4 (Figure 9A−C). The IAST selectivities indicated that the 22 and 30 Å pore size silicas had a much greater selectivity of H_2S over CH_4 (S_{H_2S/CH_4} > 250). The 60 Å pore size silica showed a higher selectivity for H_2S over CH_4 (S_{H_2S/CH_4} > 8); however, it was not as great as the other silicas. The increased silanol concentration could explain this difference, as it was shown in Figure 8 that increasing the silanol concentration had a more significant impact on the affinity of H_2S to the surface than CH_4.

Comparing the total amount adsorbed between the silica gels (Figure 9D) shows that the larger pore volume silica (60 Å pore size) had a greater total amount adsorbed than the other silicas due to the larger available volume for molecules to occupy. Interestingly, the multicomponent adsorption of the 22 Å pore size silica shows some competition between H_2S and CO_2. The 22 Å pore size silica showed higher selectivity for H_2S over CO_2 (S_{H_2S/CO_2} > 4.5). The 30 Å pore size silica showed little competition between H_2S and CO_2, with a H_2S selectivity (S_{H_2S/CO_2} > 52) an order of magnitude greater than the 22 and 60 Å pore size silicas. The 60 Å pore size silica showed the lowest selectivities of the three silicas.

Data on the adsorption of sour gas components can be used in modeling applications to estimate multicomponent behavior. The IAST model was used in this work to estimate the adsorption of a $CH_4/CO_2/H_2S$ mixture at various pressures. The IAST model is often insufficient for modeling at higher

https://doi.org/10.1021/acsomega.3c01366
ACS Omega 2023, 8, 12592−12602

pressures or in systems where the strength of the intermolecular forces of the adsorbates are too dissimilar.[26−28] While the IAST calculations agree with the correlations in Figure 7, there are no experimental multicomponent adsorption results to validate the IAST calculations.

This work demonstrated that changes in silanol concentration of the silica surface impact the adsorption of natural gas components beyond water. Specifically, H_2S was most influenced by changes in the silanol concentrations. Multicomponent modeling by IAST demonstrated that as the silanol concentration increased, so did the adsorption of H_2S. Interestingly, the silica with the intermediate concentration of silanol groups (the 30 Å pore size silica) had the greatest selectivity for H_2S, while the 22 Å pore size silica showed greater amounts of CO_2 adsorbing. The 60 Å pore size silica had the lowest H_2S and CO_2 selectivities of the silicas, indicating a greater adsorptive competition with CH_4.

Silica gels have been used industrially for adsorption separation since World War I.[29] The most common industrial application of silica gels is as a desiccant. This is due to a high selectivity toward water over other compounds and a relatively low cost of production compared to other desiccants, such as zeolites.

Materials such as zeolites have a very high affinity to water, and it has been demonstrated that when water is present in multicomponent sour gas mixtures that the amounts of adsorbed H_2S and CO_2 drop significantly.[7] The adsorption of water was not accounted for in the IAST modeling as IAST is known to fail in the estimation of water adsorption when the intermolecular forces of other adsorbates are weaker (i.e., CH_4 and CO_2).[24] The multicomponent adsorption model proposed by Wynnyk has successfully estimated high-pressure adsorption equilibria of sour gas on zeolites 4A and 13X, but the model did not do well for calculating the adsorption on silica gel.[14] The optimization of models, such as Wynnyk's model, requires experimental multicomponent adsorption data to validate the model. Unfortunately, for this work, the multicomponent adsorption of sour gas components could not be collected and is left for future studies.

3. CONCLUSIONS

It is known that the adsorption of water on silica gels is primarily affected by the concentration of silanol groups on the silica surface. However, the role of silanol groups on the adsorption of other adsorbates is less studied. This work presents adsorption isotherms for CH_4, CO_2, and H_2S on 22 and 30 Å pore size silica gels at T = 0, 25, and 50 °C. The isosteric heats of adsorption for CH_4, CO_2, H_2S, and H_2O on the 22 and 30 Å pore size silica gels and a third 60 Å pore size silica gel were compared to the total silanol concentration of the silica gels. It was found that the molecules with stronger intermolecular forces (hydrogen bonding and polarizability; H_2O and H_2S) had a more significant dependence on the silanol surface concentration than the molecule with weaker interactions (CH_4). The comparison of adsorption on the surface of the three silica gels showed that for CH_4 at low pressures (p < 10 bar) that there was no significant difference between the three silica gels. However, H_2S adsorption at low surface coverage was higher on silica gels with a higher silanol concentration. Multicomponent modeling by IAST showed that silica gels with a higher silanol concentration had a greater H_2S/CH_4 selectivity, while the silanol with the lowest concentration of silanol groups showed the lowest H_2S and CO_2 selectivities of the silicas. These results shed light on the interactions of molecules such as H_2S on the surface of silica gels and how the surface concentrations of silanol groups can affect the adsorption of sour gas components.

4. METHODS

4.1. Materials. For these experiments, CO_2 (Laser grade, 99.9995%), CH_4 (99.999%), H_2S (99.6%), and nitrogen (N_2, 99.998%) were purchased from Praxair Canada Inc. (Mississauga, Ontario, Canada). Helium (He, 99.9990%, Alphagaz 1) was purchased from Air Liquide. Gas purities were confirmed by gas chromatography (TCD/FID and SCD). Two silica gels (22 Å pore size silica gel, high purity, Davisil Grade 12, 28−200 mesh; 30 Å pore size silica gel, high purity, Davisil Grade 923, 100−200 mesh) were purchased from Sigma-Aldrich. A third silica gel (60 Å pore size silica gel: high purity, Davisil Grade 9385, 130−270 mesh) was purchased from Merck. The silica gel materials were used without modification.

4.2. Safety Considerations. The volumetric adsorption apparatus used to collect CH_4, CO_2, and H_2S was designed to operate with high-pressure H_2S. The adsorption instrument was located inside a walk-in bay equipped with wall-mounted gas detectors, high-velocity ventilation, and a caustic scrubbing system to absorb H_2S during the depletion of the instrument.

4.3. Material Characterization. The silica gels' specific surface area and pore size distribution were characterized by N_2 physisorption using a 3Flex (Micromeritics) instrument. The silica gels were degassed at T = 150 °C under a vacuum of $p = 1.33 \times 10^{-7}$ bar for at least 12 h. Scanning electron microscopy imaging was conducted with an FEI quanta 250 FEG scanning electron microscope equipped with a GATAN monoCL4 detector. DRIFT spectroscopy was conducted on the silica gels by an FT-IR spectrometer with a diffuse reflectance accessory using Resolutions Pro software. For all DRIFT experiments, samples were placed in a vacuum oven at T = 100 °C for 24 h and then promptly mixed with potassium bromide (KBr) in a 0.02:0.98 sample/KBr mass ratio.

As discussed in the previous literature, the silanol group characterization was carried out using a continuous flow thermogravimetric analyzer (SETARAM LABSYS evo) with a He flow (10 mL min^{-1}).[3,15] Following was the temperature program:

(i) the sample was equilibrated at T = 25 °C for 2 h,
(ii) the system was heated at 5 °C min^{-1} until a temperature of T = 200 °C was reached and then the temperature was maintained for 2 h,
(iii) the system was heated at 5 °C min^{-1} until a temperature of T = 400 °C was reached and then the temperature was maintained for 2 h, and
(iv) the system was heated at 5 °C min^{-1} until a temperature of T = 1000 °C was reached and then the temperature was maintained for 2 h.

The mass lost below T = 200 °C was attributed to physisorbed water on the silica gels, mass lost in the range of T = 200−400 °C was attributed to water released due to the condensation of vicinal silanol groups and the mass lost in the range of T = 400−1000 °C was attributed to water released due to the condensation of isolated and geminal silanol groups.[30]

4.4. Manometric Adsorption. The CH_4, CO_2, and H_2S adsorption isotherms were measured using an in-house-built

https://doi.org/10.1021/acsomega.3c01366
ACS Omega 2023, 8, 12592−12602

manometric adsorption instrument, which has been reported elsewhere (Figure 10).[9,14,31−33] The adsorption isotherms were

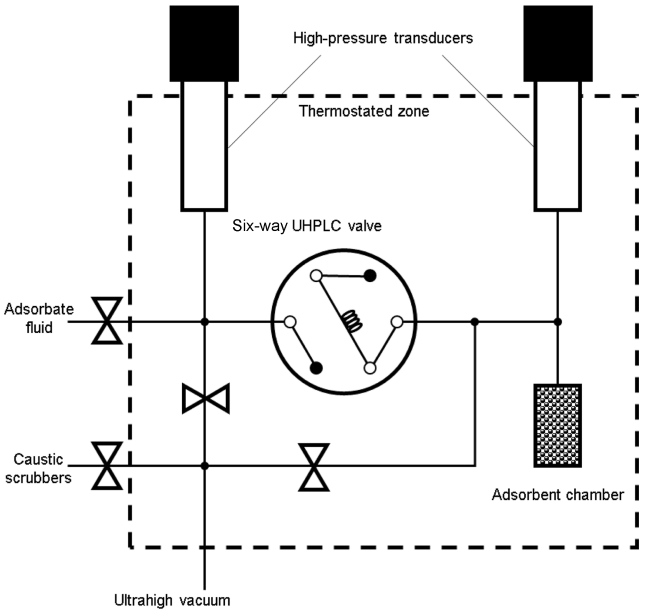

Figure 10. Schematic of the manometric adsorption instrument, adapted from the work of Wynnyk et al.[31] UHPLC stands for ultra-high-pressure liquid chromatography.

collected at T = 0.000 ± 0.005, 25.000 ± 0.005, and 50.000 ± 0.005 °C. The silica gels were activated at T = 150 °C under an ultra-high vacuum ($p = 1 \times 10^{-10}$ bar) for at least 12 h between isotherms.

All fluid thermodynamic properties were calculated by the appropriate equation of state (CO_2,[34] CH_4,[35] H_2S,[36] H_2O,[37] and He[38]) as provided within the Reference Fluid Thermodynamic and Transport Properties V9.1 (REFPROP, NIST).[39]

During the adsorption experiments, the system's temperature, the pressure of the adsorption cell (p_{ads}, bar), and the pressure of the reference cell (p_{ref}, bar) were measured. The number of moles introduced (n^{int}, mol) to the adsorption cell was calculated by multiplying the difference in density of the adsorption cell (ρ_{ads}, mol L^{-1}) and the reference cell (ρ_{ref}, mol L^{-1}) by the dosing loop volume (V_{dose}, cm^3), eq 1. The amount adsorbed (n^{ads}, mol) was then calculated by eq 2.

$$n^{int} = (\rho_{ref} - \rho_{ads}) \times V_{ref} \tag{1}$$

$$n^{ads} = \sum_{0}^{m} n^{int} - \rho_{ads} \times V_{void} \tag{2}$$

The void volume (V_{void}, cm^3) can be calculated by either helium expansion for excess adsorption or multiplying the adsorbent's mass by the adsorbent's crystal density (ρ_{crys}, g cm^{-3}). The crystal density can be calculated for amorphous materials by taking the inverse sum of the bulk material volume (V_{bulk}, cm^3 g^{-1}) and the adsorbent pore volume (V_{pore}, cm^3 g^{-1}), as described in eq 3.

$$\rho_{crys} = \frac{1}{V_{bulk} + V_{pore}} \tag{3}$$

The uncertainty of the manometric experiments was determined for n^{ads} at each recorded pressure by the propagation of random error. The uncertainties for the 95% confidence interval are reported in the Supporting Information.

4.5. Adsorption Isotherms. The modified Tóth equation (eq 4) was used with fugacity (f, bar) instead of partial pressure to model the adsorption isotherms.[40]

$$n^{ads} = \frac{n^{\infty} b f}{(1 + b f^{t})^{1/t}} + n^{\infty} \times b^{\circ} \times f \tag{4}$$

where n^{∞} (mmol g^{-1}) is the infinite capacity, b (bar^{-1}) is the affinity parameter, t (unitless) is a heterogeneity parameter, and b° (bar^{-1}) is the infinite adsorption parameter which contributes to Henry's constant. Both b and t have a temperature dependence, shown in eqs 5 and 6.

$$b = b^{\circ} \times \exp\left(\frac{-\Delta_a H}{RT}\right) \tag{5}$$

$$t = A + BT \tag{6}$$

where $\Delta_a H$ (kJ mol^{-1}) is the isosteric heat of adsorption and A (unitless) and B (K^{-1}) are empirical parameters. Here, B corresponds to a constant change in heat capacity. The isosteric heat of adsorption was determined by the methods described in the following section. The value used in the modified Tóth equation was the averaged isosteric heat over the measured loading.

The modified Tóth equation was fit to the experimental data by minimizing the mean summed square error.

4.6. Isosteric Heat of Adsorption. The isosteric heat of adsorption ($\Delta_a H$) was calculated using the equations of Titoff and Hückel from the absolute amount adsorbed.[41] The methods of Defay et al. are used in this work,[42] where $\Delta_a H$ is estimated by calculating the pure component fugacity for the corresponding absolute amount adsorbed at different temperatures, eq 7.

$$\Delta_a H = -RT\left(\frac{\partial \ln(f)}{\partial T}\right)_{n^{ads}} \tag{7}$$

A least-squares regression is used to obtain the slope for the fugacities at T = 0.000 ± 0.005, 25.000 ± 0.005, and 50.000 ± 0.005 °C. The fugacities were calculated via a cubic spline fit and were only interpolated within the measured data and were not extrapolated. Note that using a spline fit provides a more direct measurement with respect to surface loading (along with standard deviation), versus eq 5, which assumes a constant enthalpy according to the isotherm. From the resulting $\Delta_a H$ versus n^{ads} plot, a linear regression was fit and used to determine the $\Delta_a H$ at n^{ads} = 0. In addition, interpolations were made for comparison at n^{ads} = 1.5 mmol g^{-1}, which is within the majority of the experimental points for all adsorbates.

4.7. Ideal Adsorbed Solution Theory Calculations. The multicomponent adsorption calculations were conducted using the IAST theory of Myers and Prausnitz.[22] The IAST model works by defining the fugacity of component i as the adsorbate mole fraction (x_i) multiplied by a hypothetical pure component fugacity (f_i°, bar) that gives an equivalent spreading pressure (π) for all components in the mixture. Note that for this work fugacity was used instead of pressure.

$$f_i = x_i f_i^{\circ}(\pi) \tag{8}$$

The spreading pressures were defined by eq 9, where y_i is the adsorptive mole fraction. The integral presented in eq 9 does not have an analytical solution when the pure component

https://doi.org/10.1021/acsomega.3c01366
ACS Omega 2023, 8, 12592−12602

adsorption isotherm is defined by the modified Tóth equation. To solve the integral for the spreading pressures, the algorithm proposed by Do was used to iteratively solve the IAST model.[23] The initial estimate for the spreading pressure was determined using the analytical solution for the Langmuir equation to eq 9 (eq 10), where the n_i^{∞} and b_i values were obtained from the modified Tóth equation of species i.

$$\frac{\pi A}{RT} = \sum_{i=1}^{N} \int_0^{f_i} \frac{n_i^{\text{ads}}}{f_i} \, \mathrm{d}f_i \tag{9}$$

$$\frac{\pi A}{RT} = n_i^{\infty} \ln(1 + b_i f_i^{\circ}) \tag{10}$$

The selectivity between components i and j ($S_{i/j}$) for the multicomponent adsorption was calculated as the ratio of partition coefficients (K_i) for components i and j.

$$S_{i/j} = \frac{K_i}{K_j} = \frac{(n_i/y_i)}{(n_j/y_j)} \tag{11}$$

■ ASSOCIATED CONTENT

Supporting Information

The Supporting Information is available free of charge at https://pubs.acs.org/doi/10.1021/acsomega.3c01366.

Tabulated adsorption data (PDF)

■ AUTHOR INFORMATION

Corresponding Author

Robert A. Marriott − *Department of Chemistry, University of Calgary, Calgary AB T2N 1N4, Canada;* orcid.org/0000-0002-1837-8605; Email: rob.marriott@ucalgary.ca

Authors

John H. Jacobs − *Department of Chemistry, University of Calgary, Calgary AB T2N 1N4, Canada;* orcid.org/0000-0002-9286-7562

Kaylan H. McKelvie − *Department of Chemistry, University of Calgary, Calgary AB T2N 1N4, Canada*

Safeer Nanji − *Department of Chemistry, University of Calgary, Calgary AB T2N 1N4, Canada*

Complete contact information is available at: https://pubs.acs.org/10.1021/acsomega.3c01366

Notes

The authors declare no competing financial interest.

■ ACKNOWLEDGMENTS

The funding for this research was provided through the Natural Science and Engineering Research Council of Canada (NSERC) and Alberta Sulphur Research Ltd. (ASRL) Industrial Research Chair in Applied Sulfur Chemistry. In addition to NSERC, the authors are grateful to the feedback from the member companies of ASRL.

■ REFERENCES

(1) *Gas Processors Supplier's Assoc. (GPSA)*, Engineering Data Book; Tulsa, OK, 1987.

(2) A Christy, A. Effect of Heat on the Adsorption Properties of Silica Gel. *Int. J. Eng. Technol.* **2012**, *4*, 484−488.

(3) Saliba, S.; Ruch, P.; Volksen, W.; Magbitang, T. P.; Dubois, G.; Michel, B. Combined Influence of Pore Size Distribution and Surface Hydrophilicity on the Water Adsorption Characteristics of Micro- and Mesoporous Silica. *Microporous Mesoporous Mater.* **2016**, *226*, 221−228.

(4) Alcañiz-Monge, J.; Pérez-Cadenas, M.; Lozano-Castelló, D. Influence of Pore Size Distribution on Water Adsorption on Silica Gels. *J. Porous Mater.* **2010**, *17*, 409−416.

(5) Marriott, R. A.; Pirzadeh, P.; Marrugo-Hernandez, J. J.; Raval, S. Hydrogen Sulfide Formation in Oil and Gas. *Can. J. Chem.* **2016**, *94*, 406−413.

(6) Kim, K. C.; Jang, S. S. Molecular Simulation Study on Factors Affecting Carbon Dioxide Adsorption on Amorphous Silica Surfaces. *J. Phys. Chem. C* **2020**, *124*, 12580−12588.

(7) Steuten, B.; Pasel, C.; Luckas, M.; Bathen, D. Trace Level Adsorption of Toxic Sulfur Compounds, Carbon Dioxide, and Water from Methane. *J. Chem. Eng. Data* **2013**, *58*, 2465−2473.

(8) Mohammed, S.; Sunkara, A. K.; Walike, C. E.; Gadikota, G. The Role of Surface Hydrophobicity on the Structure and Dynamics of CO_2 and CH_4 Confined in Silica Nanopores. *Front. Clim.* **2021**, *3*, 713708.

(9) Wynnyk, K. G.; Hojjati, B.; Marriott, R. A. Sour Gas and Water Adsorption on Common High-Pressure Desiccant Materials: Zeolite 3A, Zeolite 4A, and Silica Gel. *J. Chem. Eng. Data* **2019**, *64*, 3156−3163.

(10) Adeniyi, K. I.; Wan, H. H.; Deering, C. E.; Bernard, F.; Chisholm, M. A.; Marriott, R. A. High-Pressure Hydrogen Sulfide Experiments: How Did Our Safety Measures and Hazard Control Work during a Failure Event? *Safety* **2020**, *6*, 15.

(11) Thommes, M.; Kaneko, K.; Neimark, A. V.; Olivier, J. P.; Rodriguez-Reinoso, F.; Rouquerol, J.; Sing, K. S. W. Physisorption of Gases, with Special Reference to the Evaluation of Surface Area and Pore Size Distribution (IUPAC Technical Report). *Pure Appl. Chem.* **2015**, *87*, 1051−1069.

(12) Zhuravlev, L. T. The Surface Chemistry of Amorphous Silica. Zhuravlev Model. *Colloids Surf., A* **2000**, *173*, 1−38.

(13) Cappeletti, L. B.; Moncada, E.; Poisson, J.; Butler, I. S.; Santos, J. H. Z. D. Determination of the Network Structure of Sensor Materials Prepared by Three Different Sol-Gel Routes Using Fourier Transform Infrared Spectroscopy (FT-IR). *Appl. Spectrosc.* **2013**, *67*, 441−447.

(14) Wynnyk, K. G. High-pressure Adsorption Equilibria Aimed at Optimizing Sour Gas Conditioning. Ph.D. Dissertation, University of Calgary, Calgary, Alberta, Canada, 2019.

(15) Jacobs, J. H.; Deering, C. E.; Sui, R.; Lesage, K. L.; Marriott, R. A. Degradation of Desiccants in Temperature Swing Adsorption Processes: The Temperature Dependent Degradation of Zeolites 4A, 13X and Silica Gels. *Chem. Eng. J.* **2023**, *451*, 139049.

(16) Wang, Y.; LeVan, M. D. Adsorption Equilibrium of Binary Mixtures of Carbon Dioxide and Water Vapor on Zeolites 5A and 13X. *J. Chem. Eng. Data* **2010**, *55*, 3189−3195.

(17) Demir, H.; Mobedi, M.; Ülkü, S. Microcalorimetric Investigation of Water Vapor Adsorption on Silica Gel. *J. Therm. Anal. Calorim.* **2011**, *105*, 375−382.

(18) Chakraborty, A.; Saha, B. B.; Koyama, S.; Ng, K. C.; Srinivasan, K. Adsorption Thermodynamics of Silica Gel−Water Systems. *J. Chem. Eng. Data* **2009**, *54*, 448−452.

(19) de Lange, R. S. A.; Hekkink, J. H. A.; Keizer, K.; Burggraaf, A. J.; Ma, Y. H. Sorption Studies of Microporous Sol-Gel Modified Ceramic Membranes. *J. Porous Mater.* **1995**, *2*, 141−149.

(20) Kennedy, D. A.; Mujcin, M.; Trudeau, E.; Tezel, F. H. Pure and Binary Adsorption Equilibria of Methane and Nitrogen on Activated Carbons, Desiccants, and Zeolites at Different Pressures. *J. Chem. Eng. Data* **2016**, *61*, 3163−3176.

(21) Shen, Y.; Shi, W.; Zhang, D.; Na, P.; Fu, B. The Removal and Capture of CO_2 from Biogas by Vacuum Pressure Swing Process Using Silica Gel. *J. CO2 Util.* **2018**, *27*, 259−271.

(22) Tan, S. J.; Do, D. D.; Chew, J. W. The Physisorption Mechanism of SO_2 on Graphitized Carbon. *Phys. Chem. Chem. Phys.* **2020**, *22*, 21463−21473.

(23) Liu, L.; Tan, S.; Do, D. D. Computer Simulation and Experimental Studies of Various Environmental Gases (NH_3, CH_2O, SO_2, H_2S, Benzene, Water) on Carbon Materials. In *Porous Materials*; Moreno-Piraján, J. C., Giraldo-Gutierrez, L., Gómez-Granados, F., Eds.; Springer International Publishing: Cham, 2021; pp 79−111.
(24) Kim, H. J.; Jeon, H.; Shin, Y.-H. H_2S Adsorption Process on (0001) α -Quartz SiO_2 Surfaces. *J. Appl. Phys.* **2018**, *124*, 115301.
(25) Myers, A. L.; Prausnitz, J. M. Thermodynamics of Mixed-Gas Adsorption. *AIChE J.* **1965**, *11*, 121−127.
(26) Do, D. D. *Adsorption Analysis: Equilibria and Kinetics*; Series on chemical engineering; Imperial College Press: London, 1998.
(27) Walton, K. S.; Sholl, D. S. Predicting Multicomponent Adsorption: 50 Years of the Ideal Adsorbed Solution Theory. *AIChE J.* **2015**, *61*, 2757−2762.
(28) Jacobs, J. H.; Chou, N.; McKelvie, K. H.; Commodore, J. A.; Sui, R.; Lesage, K. L.; Wynnyk, K. G.; Xiao, Y.; Biesinger, M. C.; Hill, J. M.; Marriott, R. A. Screening Activated Carbons Produced from Recycled Petroleum Coke for Acid Gas Separation. *Carbon Trends* **2023**, *10*, 100243.
(29) Ruthven, D. M. *Principles of Adsorption and Adsorption Processes*; Wiley: New York, 1984.
(30) Nawrocki, J. The Silanol Group and Its Role in Liquid Chromatography. *J. Chromatogr. A* **1997**, *779*, 29−71.
(31) Wynnyk, K. G.; Hojjati, B.; Pirzadeh, P.; Marriott, R. A. High-Pressure Sour Gas Adsorption on Zeolite 4A. *Adsorption* **2017**, *23*, 149−162.
(32) Wynnyk, K. G.; Hojjati, B.; Marriott, R. A. High-Pressure Sour Gas and Water Adsorption on Zeolite 13X. *Ind. Eng. Chem. Res.* **2018**, *57*, 15357.
(33) Jacobs, J. H.; Wynnyk, K. G.; Lalani, R.; Sui, R.; Wu, J.; Montes, V.; Hill, J. M.; Marriott, R. A. Removal of Sulfur compounds from Industrial Emission Using Activated Carbon Derived from Petroleum Coke. *Ind. Eng. Chem. Res.* **2019**, *58*, 18896−18900.
(34) Span, R.; Wagner, W. A New Equation of State for Carbon Dioxide Covering the Fluid Region from the Triple-Point Temperature to 1100 K at Pressures up to 800 MPa. *J. Phys. Chem. Ref. Data* **1996**, *25*, 1509−1596.
(35) Setzmann, U.; Wagner, W. A New Equation of State and Tables of Thermodynamic Properties for Methane Covering the Range from the Melting Line to 625 K at Pressures up to 100 MPa. *J. Phys. Chem. Ref. Data* **1991**, *20*, 1061−1155.
(36) Lemmon, E. W.; Span, R. Short Fundamental Equations of State for 20 Industrial Fluids. *J. Chem. Eng. Data* **2006**, *51*, 785−850.
(37) Wagner, W.; Pruß, A. The IAPWS Formulation 1995 for the Thermodynamic Properties of Ordinary Water Substance for General and Scientific Use. *J. Phys. Chem. Ref. Data* **2002**, *31*, 387−535.
(38) Ortiz Vega, D. O. A new wide range equation of state for helium-4. Ph.D. Dissertation, Texas A & M University, 2013.
(39) Lemmon, E. W.; Bell, I. H.; Hubaer, M. L.; McLinden, M. O.; NIST. *Reference Fluid Thermodynamics and Transport Properties - REFPROP*; National Institute of Standards and Technology: Gaithersburg, 2013.
(40) Tóth, J. State Equations of the Solid-Gas Interface Layers. *Acta Chim. Acad. Sci. Hung.* **1971**, *69*, 311−328.
(41) Hückel, E. Theory of Heat Evolved in Capillary Condensation. *Trans. Faraday Soc.* **1932**, *28*, 382−386.
(42) Defay, R.; Prigogine, I.; Bellemans, S.; Everett, D. H. *Surface Tension and Adsorption*; Longmans: London, 1966.

https://doi.org/10.1021/acsomega.3c01366
ACS Omega 2023, 8, 12592−12602